Electron Irradiation of Gold Below 2 K*

P. S. Gwozdz and J. S. Koehler
Department of Physics, University of Illinois, Urbana, Illinois 61801
(Received 6 April 1973)

Gold (99.9999% purity) was irradiated by 2.5-MeV electrons below 2 K. Damage production was monitored by measuring the dc resistivity of the gold. The production rate $d\rho/d\Phi$ (change in resistivity per integrated electron flux) was found to (a) be enhanced by the presence of quenched vacancies at extremely low values of integrated flux, (b) be attenuated by the presence of quenched vacancies at higher values of integrated flux, (c) decrease with increasing Φ particularly at the lowest values of Φ, and (d) increase with increasing $d\Phi/dt$ (beam flux). Thermal recovery of resistivity was observed as low as 2.3 K. The recovery in the range 2.3–30 K was found to (a) be enhanced by the presence of quenched vacancies, (b) be attenuated by the presence of silver impurities, and (c) increase with increasing Φ. These observations are consistent with the hypothesis that the interstitial in gold undergoes long-range migration either during electron irradiation at 1.7 K or during annealing at 1.95 K.

I. INTRODUCTION

From the earliest low-temperature irradiations[1–3] recovery of radiation damage in gold has differed significantly from that in copper and silver. In the latter two materials, low-temperature recovery (stage I) is characterized[1,4,5] by abrupt drops in resistivity above 13 K. These drops are attributed to the recombination of various close Frenkel pairs and to the migration of interstitials. In gold, on the other hand, resistivity recovers slowly and more or less continuously even from the lowest temperature reported.[6] In a recent review,[7] the interpretation of the low-temperature recovery in gold was left open. The present experiment represents an attempt to find the lowest temperature at which the gold interstitial undergoes long-range migration. It will be shown that such migration occurs either during electron irradiation at 1.7 K or during annealing at 1.95 K. Low-temperature interstitial migration has been proposed earlier to explain radiation damage in silicon at 1.6[8] and 0.5 K.[9]

II. EXPERIMENTAL DESCRIPTION

A. Sample Preparation

Gold was purchased from Cominco in the form of 375-μm sheets. The starting material was 6-9's grade; mass-spectrographic analysis before rolling into sheets showed $\leqq 0.1$ ppm each of Ca, Cu, Mg, Si, and Ag. The sheets were cut into samples of the form in Fig. 1(a) using an electric-discharge machine. Burrs on the cut edges were removed manually using a sharp knife edge. Samples were then etched in boiling aqua regia to remove nominally 50 μm of surface material. All samples were annealed 3 h at 900 °C in an air furnace. Mounting was done using a 6-μm Mylar insulating film and a thin coating of GE 7031 varnish. After mounting and baking, the support strips were manually cut away with a blade to produce the sample shown in Fig. 1(b); current and potential leads were soldered to the four tabs shown.

Gold was also purchased with 0.01 and 0.1 at.% silver doping and prepared in the same way. Quenched samples were annealed in a vertical furnace and drop quenched into brine; a quick-set epoxy was used for mounting to provide a firm attachment to the Mylar films (for strip cutting) without baking.

The geometrical factor (cross-sectional area/

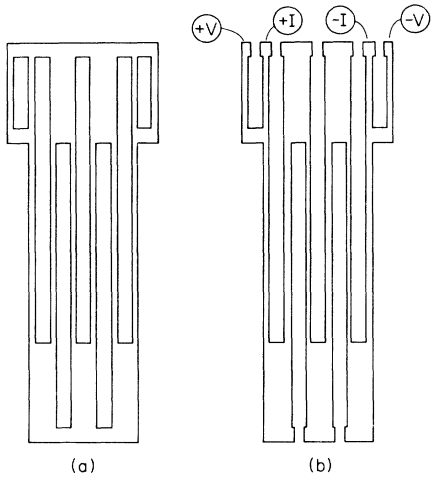

FIG. 1. Sample design. Over-all dimensions 3.556 × 1.295 cm. Thickness 0.375 mm before etching. All strips 0.425 mm wide before etching. (a) Sample with support strips as cut by EDM. (b) Sample after etching, annealing, and mounting with support strips cut away. Current and potential tabs indicated.

TABLE I. The eight samples used in the four runs. The geometrical factor A/l was obtained from liquid-nitrogen measurements of the sample resistance and from the sample resistance at 1.7 K. All annealed 3 h at 900 °C before preparation.

Sample	Impurity (at.%)	Preparation	$\rho(22\,°C)/\rho(2\,K)$ No size correction	$\rho(2\,K)$ $10^{-9}\,\Omega$ cm	A/l (10^{-4} cm)	Irradiation
I A	0.0005	slowly cooled	4407	0.5531	0.7415	$I_A I_Q$ irrad together
I Q	0.0003	quenched 900 °C to brine − 5 °C	313	6.735	0.7294	$I_A I_Q$ irrad together
II L	0.0001	slowly cooled	7205	0.3383	1.9415	low dose
II H		slowly cooled	7223	0.3375	1.747	high dose
III A		slowly cooled	6354	0.3837	1.4645	III_A, III_Q irrad separately
III Q		quenched 600 °C to brine − 5 °C	1412	1.726	1.954	to identical dose
IV 0.01Ag	0.01	slow cool	752	3.243	1.827	$IV_{0.01}$, $IV_{0.1}$ irrad separately
IV 0.1Ag	0.1	slow cool	89.1	27.35	1.720	to identical dose

length) was obtained for each sample by measuring the resistance at liquid-nitrogen temperature (minus residual resistance for quenched and doped samples) and using 0.478 $\mu\Omega$ cm for the resistivity. The irradiated region ($\frac{2}{3}$ of the total sample length) consisted of 6 strips of 1.27 cm length; these geometrical factors are given in Table I. The fact that liquid-nitrogen temperature is uncertain to ±0.04% introduces a relative uncertainty of ±0.07% in the geometrical factors.

The familiar thermal contribution to the resistivity (linear at high temperatures, about T^5 at low temperatures) follows the Grüneisen formula.[10] At very low temperatures, resistivity is dominated by the temperature-independent residual resistivity, mostly due to size effects in pure samples, due to impurities, quenched vacancies, and radiation damage in others. In this experiment, the thermal contribution could be followed down to 2 K; all resistivity measurements were done well below 2 K except when indicated otherwise. The ratios of room (22 °C) to residual resistivity for various specimens are given in Table I.

After irradiation, samples from run I were analyzed by the University of Illinois Materials Research Laboratory's Spectrographic Lab and found to contain localized Fe contamination of 3–9 ppm. In subsequent runs, all handling by metal tools after etching was eliminated; mass-spectrographic analysis of run-II samples showed improved purity (Table I).

Room-temperature annealing of quenched samples always showed (50–80)% recovery, indicating the migration of quenched vacancies to vacancy clusters and other sinks.

B. Cryostat

1. Dewar

The 10-liter commercial dewar (A) and the vacuum housing (B) are shown in Fig. 2(a). Also shown are the electrical and plumbing connections. In particular, the six potential leads (Q_a) (two to each of the two gold samples, two to the sample thermometer) are threaded through a tube (N) to prevent excessive cold working during assembly and to minimize thermal fluctuations (see Sec. II D). All connections to these wires are with pure copper crimp connectors on gold-plated copper thermal posts with grounded draft shielding.

In Fig. 2(b) the locations of the refrigerator assembly (R) and of the sample chamber (S) are indicated. Also shown schematically are the cryogenic liquids and the radiation shields.

2. Refrigerator

Details of the He^4 refrigerator (R) built for this experiment are shown in Fig. 3. When opened, the needle valve (R_b) allows liquid helium at atmospheric pressure to flow from the Dewar above. The impedance tube (X), seen in detail in Fig. 4, is 3.5 cm long. It was made by threading a No. 24 (0.5 mm diameter) chromel A wire (X_d) into a cupronickel capillary tube (0.8 mm o.d. × 75-μm wall) (X_c). After a few days of use, the impedance of the tube increases, probably due to the accu-

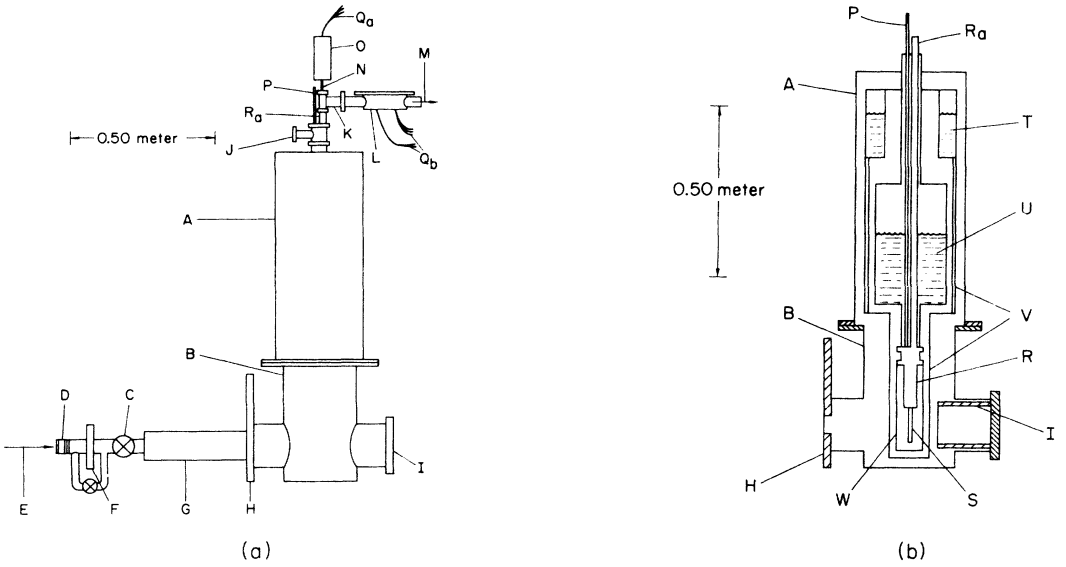

FIG. 2. Complete cryostat assembly. (a) Full view, (b) cross section. *A*, Commercial helium Dewar with 10-liter capacity, with 5.08-cm neck, with 5.08-cm open tail, and with side flange for diffusion pump (not shown); *B*, vacuum housing with vacuum common to Dewar; *C*, gate valve; *D*, flange to accelerator; *E*, beam direction; *F*, flange containing 50-μm aluminum scattering foil; *G*, drift tube; *H*, radiation shield, insulated from vacuum housing; *I*, Faraday cup, insulated from vacuum housing; *J*, atmospheric vent manifold for helium Dewar; *K*, refrigerator manifold thermally isolated from the vent manifold by the stainless-steel pump out tube (R_a); *L*, wire can for vacuum feedthrough of all wires except potential leads; *M*, direction to helium pump; *N*, tube for thermal isolation from refrigerator manifold and for protection of potential leads from thermal irregularities (extends well into Dewar); *O*, grounded draft shield protecting gold-plated copper thermal post for attachment of potential leads; *P*, needle valve; *Q*, wires; *R*, outline of refrigerator assembly with wires (not shown) inside pump out tube (R_a); *S*, outline of sample chamber; *T*, liquid N_2; *U*, liquid He; *V*, 78-K radiation shiled; *W*, 4.2-K radiation shield.

mulation of solid air; 8 A of current can be passed through the heater wire (X_g), using the impedance tube as its own resistive heater and the cryostat as a current return. The shield tube (X_e) minimizes radiation heating of the superfluid helium bath; in this way, the solid air can be boiled off. The impedance tube can thus be restored to its original flow rate without heating the bath above 1.7 K.

A 26-liter per second pump is used to pump on the liquid helium. Gas flow is limited by the conductance of the 1.9-cm diameter pump-out tube (R_a) at the top (near room temperature). Refrigerator temperature during filling is 1.7–1.9 K, depending upon how much the needle valve is opened. Temperature with the needle valve closed is 1.3 K, falling with time to 1.2 K as the liquid boils off, reducing superfluid film creep up the sides of the reservoir. Total time for filling is 4 min; total time for boiloff of a full reservoir is 5 h. A very slight opening of the needle valve allows a reduced flow of helium to overfill the reservoir so that it tries unsuccessfully to cool the Dewar above. The refrigerator can be left unattended in this condition for a few days; it maintains 1.45 ± 0.05 K.

The stainless-steel spacer (R_f) is for thermal isolation; the reservoir (R_i) is of gold-plated copper. All the pieces shown in Fig. 3 are connected by indium O-ring seals, e.g., (S_g) seen both in Fig. 3 and in Fig. 5. The rectangular flanges with four screws are not visible in the cross sections. The thermal binding posts are of gold-plated copper. The upper one (R_g) is in thermal contact with the Dewar above (4.2 K); all wires are wound and varnished to it. The lower one (R_h) is drilled to accomodate four Mylar-coated gold-plated copper posts, which are varnished into the drilled holes. These four threaded posts are used to make quick nonthermal contact (pure copper crimp connectors) to two Alan Bradley carbon resistors. The upper resistor (470 Ω room temperature), varnished into a drilled hole in the lower post, is used as a heater during thermal annealing. The lower resistor (200 Ω room temperature), hanging near the bottom of the reservoir and shielded from cold gas flow, experiences a slight increase in resistance when the level of superfluid helium passes through. This resistor is used as one arm of an external resistance bridge; the off-balance current is amplified to give a signal to the operator that the reservoir is low. During run I the electron beam

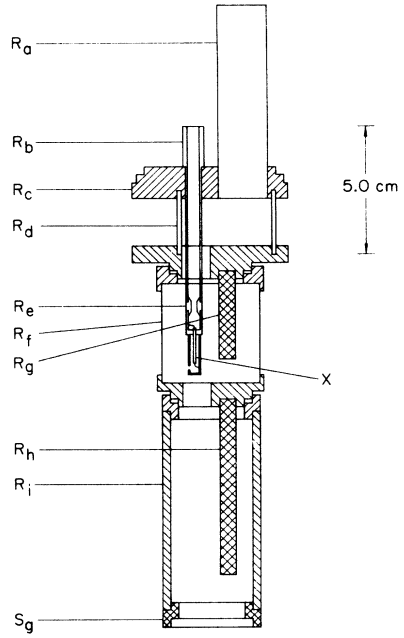

FIG. 3. Refrigerator assembly seen in cross section. (R_a) pump-out tube drawn with length greatly compressed; (R_b) needle valve drawn with threading and male piece omitted for clarity; (R_c) flange for attachment to bottom of helium Dewar; (R_d) radiation baffle piece; (R_e) valve seat; (R_f) spacer piece; (R_g) upper thermal post; (R_h) lower thermal post; (R_i) reservoir piece; (S_g) female flange for attachment of sample chamber; (X) impedance tube. The three pieces (baffle, spacer, and reservoir) are tubular with rectangular flanges for indium O-ring seals; the four screws on each flange are not seen in cross section. All material is gold-plated copper except the stainless-steel valve seat, the pump-out tube, and the spacer tube. All joints were soft soldered.

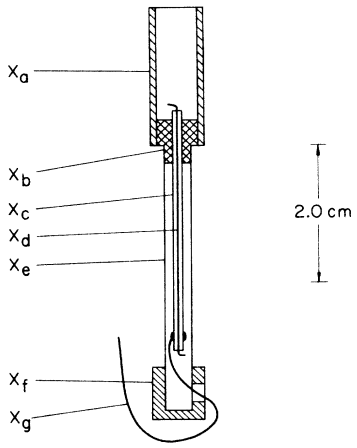

FIG. 4. Cross-sectional sketch of impedance tube. See text for dimensions. (X_a) base of needle valve; (X_b) copper plug; (X_c) cupronickel capillary tube; (X_d) chromel wire; (X_e) stainless-steel shield tube; (X_f) copper nozzle; (X_g) heater current wire. All parts soft soldered together except chromel wire left alone.

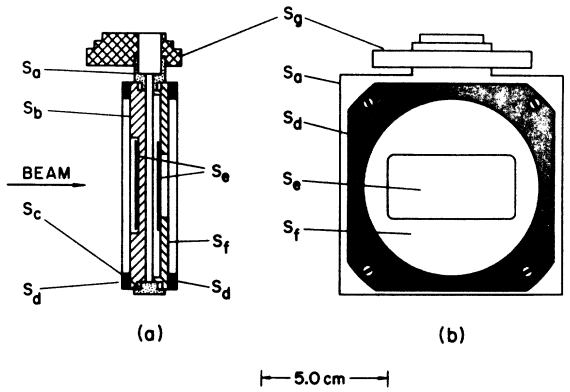

FIG. 5. Sample chamber. (a) Vertical cross section through center. (b) View looking up beam direction. (S_a) Chamber support (gold-plated copper); (S_b) sample mounting plate with two samples not visible in cross section; (S_c) 1.6 mm diameter indium O-rings (two) compressed to rectangular dimensions of grooves; (S_d) stainless-steel pressure rings (two); (S_e) aluminum-foil windows (two) with attachment plates not drawn for clarity; (S_f) cover plate; (S_g) gold-plated copper male flange, soft soldered to chamber support, for attachment to superfluid helium reservoir.

flux was adjusted to maintain bridge balance while the needle valve was very slightly open. During runs II–IV, the needle valve was closed during irradiation; at the bridge signal, the beam was magnetically bent away and the reservoir was filled by remote opening of the needle valve. Repeating this process, the irradiations were done in steps (nominally $6\times10^{14}e/\text{cm}^2$ per step).

3. Sample Region

The sample chamber is shown in Fig. 5. Details of the indium O-ring seal (S_c) used to attach the sample-mounting plate (S_b) are seen. The cover plate (S_f) is similarly attached after the cryostat leads are connected. The cover plate has a large 50-μm aluminum-foil beam exit window 6 mm from the samples. During each run, the sample chamber was kept full of superfluid helium liquid except when indicated otherwise. The 6.4-mm diameter hole at the top of the chamber leads to the helium reservoir.

The sample mounting plate (S_b) is shown in Fig. 6. Two gold samples (S_i) are shown varnished (GE 7031) to Mylar films which are varnished to the gold-plated copper mounting plate. For clarity, only four strips per sample are drawn; in fact, there are six. The mounting bars (S_m) are two nylon sheets each with four holes to clear small nylon screws used to make quick press contact between pairs of pure copper crimp connectors (one of each pair to the sample, one to the cryostat). The mounting plate (S_b) is tapped to

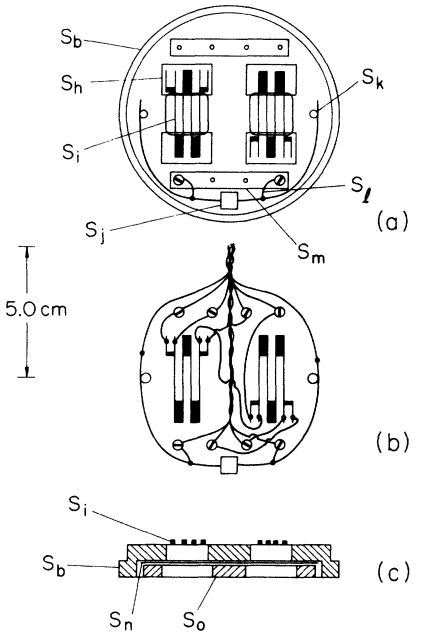

FIG. 6. Sample region. (a) View of sample before attachment of leads, looking up beam direction. (b) Sketch of electrical leads. For clarity, mounting plate is not shown. Each nylon screw makes press contact between a pair of pure copper crimp connectors, one of which is crimped to a copper wire which is soldered to a sample tab or thermometer lead, and one of which is crimped to a copper wire from the cryostat. (c) Horizontal exaggerated cross section through center of sample mounting plate. (S_b) Sample mounting plate (gold-plated copper, OFHC); (S_h) 6-μm Mylar films (four) varnished (GE 7031) to mounting plate; (S_l) gold samples (two) varnished to Mylar with only four of six actual strips per sample shown for clarity; (S_j) carbon resistance thermometer varnished into thermal post; (S_k) current leads (two) (advance alloy) from thermometer wound and varnished to posts; (S_l) potential leads (two) from thermometer; (S_m) nylon insulating bars (two); (S_n) 50-μm aluminum-foil window; (S_o) attachment plate (gold plated copper).

take the eight screws. The carbon resistance thermometer is located below the irradiation region, varnished into a drilled hole in a gold plated copper cube (S_j) which is varnished to the plate (S_b). The samples are located 3 mm from the 50-μm aluminum-foil windows (S_n), which are epoxied to the plate (S_b). The attachment plate (S_o) epoxied to the foil, seen in exaggerated cross section in Fig. 6; allows the sample chamber to be pressurized with respect to the cryostat vacuum.

C. Electron Beam

1. Homogeneity

Electrons at 2.5 MeV were provided by the University of Illinois Van der Graff generator. A 50-μm aluminum foil served to separate the generator vacuum from the cryostat vacuum and to scatter the electrons for beam homogeneity. A sketch of the collimation system is given in Fig. 7. Two collimation systems, side by side, were used, one for each sample. Shutters located just before the room-temperature collimators were used to shutter one or the other sample. With one sample closed, the beam was tuned to the other sample; opening the former sample and closing the latter reduced the measured beam by 10% (both sample beams are measured by the same Faraday cup). Electron multiple-scattering theory[11] predicts a Gaussian angular distribution of the beam with 4.9°, the angle at which the distribution has $1/e$ of its maximum value. For the 3.3-cm center-to-center separation of the two collimators, it is calculated that the beam should fall 21%; this result is in reasonable agreement with the 10% experimental figure. Calculation for the variation across a sample (6.4 mm maximum) yields 0.9%.

In summary, the beam is practically homogeneous across a given sample. In run I where both samples were irradiated together, maximum instantaneous beam discrepancy was ± 10%. In runs II–IV, samples were shuttered alternately, irradiating the samples in steps one at time.

2. Flux Measurement

As illustrated in Fig. 7, the tip of the Faraday cup makes an angle of 45° with the center of the sample chamber. The two sample-chamber beam windows are of the same thickness as the scattering foil; the 4.9° characteristic angle calculated

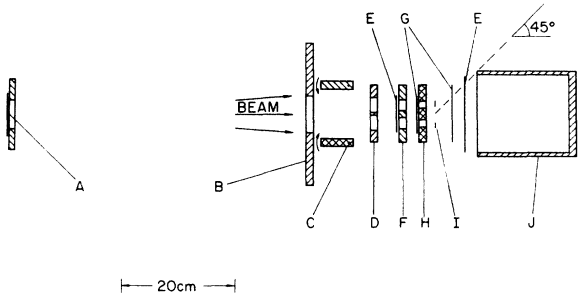

FIG. 7. Beam collimation shown to scale in horizontal cross section; *A*, 50-μm aluminum scattering foil; *B*, radiation shield; *C*, shutters (two); *D*, room-temperature collimator with two 1.9-cm squares holes; *E*, liquid-nitrogen temperature windows of 13-μm aluminum foil; *F*, liquid N_2 collimator with two 1.6-cm square holes; *G*, liquid-helium windows (4.2 K before beam heating) of 13-μm aluminum foil; *H*, liquid He collimator with two 1.27-cm square holes; *I*, two samples drawn with sample chamber omitted for clarity (chamber windows larger than liquid-He collimated beam size); *J* Faraday cup. All collimators 1.27 cm thick. All square holes aligned visually ± 2 mm.

above applies. A similar calculation can be done for the 9.55-mm beam path through superfluid helium by extrapolating the theory[11]; the resulting angle is 7.8°. For the gold samples, the characteristic angle is calculated to be 90.5°, but the gold samples are exposed to only 19% of the beam area. According to the theory, then, about 15% of the beam escapes detection. No corrections for this effect have been applied to the data; 15 ± 5% should be added to the flux of the present experiment if comparison to other experiments is desired.

3. Energy Loss

The energy loss of the 2.5-MeV electron beam in penetrating the aluminum windows and helium bath before reaching the sample is calculated[12] to be 0.12 MeV. Loss through the sample is calculated to be 0.74 MeV. The average energy in the sample is 2.01 MeV.

D. Resistivity Measurements

Standard potentiometric dc methods were used to measure sample resistivity. A Rubicon No. 2768 potentiometer was used with a Leads and Northrup No. 9838 nanovolt detector; 3-nV resolution was possible. Accuracy of measurements is discussed below in the following subsections.

1. Resolution

Variations in time of thermal emf's (due to fluctuations of helium-gas cooling of potential leads limited the resolution of potential to 5 nV; this corresponds to 1.8×10^{-13} Ω cm or 0.03% of the final irradiated resistivity for the well-annealed pure samples. For quenched and doped samples (higher resistivity), resolution was limited by the 0.01% relative accuracy with which the sample current could be adjusted. These figures apply to initial measurements and isochronal-recovery data; production-rate data were taken remotely and the corresponding figures are 10-nV thermal noise in pure samples and 0.02% accuracy in quenched and doped samples.

2. Comparison of Samples

Irradiated resistivity is determined by the geometrical factor for the irradiated region of the samples (Table I). For an ideal sample, the geometrical factor for the irradiated region is a fixed fraction ($\frac{2}{3}$ in the present experiment) of the measured total geometrical factor. For a real sample, variations in dimensions (due to variations in etch rate along the sample during preparation) may lead to erroneous geometrical factors. No such variations were noted microscopically (about 1% accuracy) except for the samples of run I (about 15% variations).

3. Comparison to Other Experiments

Absolute resistivity accuracy is determined by the absolute accuracy of the geometrical factor measurement (a few percent). In practice, comparison to other experiments is limited by flux measurements and by electron energy determination (see Sec. II C 2.)

E. Temperature Measurement

An Alan Bradley carbon resistor (200 Ω at room temperature) was used to measure the temperature of the He bath. The resistance versus temperature of the resistor was calibrated for each run by measuring the resistance at room temperature, at atmospheric liquid-nitrogen temperature and at liquid-helium temperatures at atmospheric pressure, at the λ point of liquid helium and at a few mm He pressure (vapor pressure versus temperature data).[13] Standard fitting techniques[13] were used to interpolate these points. With the electron beam and the sample current off, bath temperature varied from 1.2 to 1.3 K depending upon how full the He reservoir was (superfluid film creep). With the electron beam on at $(0.78 \pm 0.04)\times10^{12} e/\mathrm{cm}^2\,\mathrm{sec}$ (used in the latter part of run II and throughout runs III and IV), the bath temperature was 1.55 ± 0.05 K. At the highest flux obtainable ($4\times10^{12} e/\mathrm{cm}^2\,\mathrm{sec}$ used occasionally in run I) bath temperature was 1.8 K. During resistivity measurements bath temperature rose due to resistive heating of the copper leads by the sample current; currents were chosen to keep the bath temperature well below 2 K. It will now be shown both theoretically and experimentally that the sample temperature is essentially equal to the He bath temperature. It will be seen that the highest temperatures during the irradiation parts of the experiment were obtained during the filling of the helium reservoir with the electron beam off.

1. Irradiation Temperature

Sample heat $\dot{\mathcal{S}}$ by the electron beam is given by

$$\dot{\mathcal{S}} = \frac{dE}{dx}\,\dot{\Phi} V \quad . \tag{1}$$

For the energy loss dE/dx, we use[12] 1.398 MeV $\mathrm{cm}^2/\mathrm{g} = 4.327\times10^{-12} j/e$ cm; for the flux $\dot{\Phi}$ we use $0.78\times10^{12} e/\mathrm{cm}^2\,\mathrm{sec}$; and for the volume V we use the nominal dimensions of the irradiated region of the etched samples $7.62\times0.0275\times0.0408 = 8.55\times10^{-3}$ cm^3 and obtain 29 mW for the beam heating of each of the two samples mounted together. A similar calculation yields 103 mW for the bath heating and 17.2 mW for the heating of the aluminum-foil windows. In addition, a very few widely scattered electrons will contribute significant

heating if completely stopped by the material of the He reservoir; clearly the sample heating contributes less than one-third of the energy which raises the temperature of the He bath. The sample heating per unit length is 3.8 mW/cm. The problem of a round wire with uniform heating is easily solved to give the temperature difference ΔT between the center and surface:

$$\Delta T = (1/4\pi\kappa)(\dot{\mathcal{E}}/l) \quad , \tag{2}$$

where κ is the thermal conductivity and $\dot{\mathcal{E}}/l$ is the heating per unit length. Using this result for our rectangular wires with rounded edges and the handbook[14] $\kappa = 8$ W/cm K at 1.8 K gives $\Delta T = 3.78 \times 10^{-5}$ K. Using the results for a round wire is approximate; the temperature difference for a rectangular wire should be less. The handbook κ was obtained by interpolating the linear $\kappa(T)$ at 1.8 K; the quoted residual resistivity for the handbook data was 5.5×10^{-9} Ω cm (compare to Table I). This internal heating of the samples is negligible, even for the occasional use of $4 \times 10^{12} e/\text{cm}^2$ sec in run I.

The average heat flow through the sample surface is 28 mW/cm^2 from the above figures for $0.78 \times 10^{12} e/\text{cm}^2$ sec. The kapitza resistance[15] for gold at 1.8 ± 0.2 K is 1 ∓ 0.3 cm^{2}K/W. Hence the sample surface is 0.028 K warmer than the surrounding superfluid helium. This temperature difference, except for the $4 \times 10^{12} e/\text{cm}^2$ sec flux used occasionally in run I, is about the same as the errors estimated in carbon resistance thermometry.

2. Temperature during Resistivity Measurements

Sample heating by the measuring current is accurately given by current times measured potential. The results range from 0.1 mW for the pure samples of run II at 5 A to 2.2 mW for the 0.1% doped sample of run IV at 3 A. Heating due to the resistance of the copper leads and crimp copper connections, however, turns out to be large enough to heat the He bath to as much as 1.7 K. The discussion in Sec. II E 1 can be repeated with the more favorable conditions during sample measurement to show that the difference in temperature between sample and bath is negligible.

Experimentally, sample heating can be detected by the thermal contribution to the resistivity, which could be resolved as low as 2 K. The thermal contribution was checked by closing the He pump and following the resistance rise with a low measuring current. No such rise was seen when the resistance was monitored by low measuring current (0.1 A) and the electron beam was switched on and off. A slight thermal rise could be observed, however, with the beam off by increasing the measuring current to about 6 A. In addition, jumpiness appeared in the measuring current, apparently caused by local regions (near contacts or copper leads) of He liquid intermittently making the superfluid-normal transition. All measurements were done with the sample current at least 1 A lower than the minimum c rent needed to cause thermal increase or jumpiness in resistivity measurements. Thus the highest sample temperature during resistivity measurement was 1.7 K.

3. Temperature during Filling of Refrigerator

If allowed to overfill with the needle valve wide open, the refrigerator temperature rises to just above the λ point (2.17 K), at which time flow through the impedance tube (see Sec. II B) decreases significantly. Equilibrium is established at about 2.2 K. In practice, except occasionally in run I, the needle valve was closed before 2.0 K was reached; the actual highest temperature achieved varied from fill to fill.

4. Summary of Temperature and Measurement

Temperature measurements were performed on the He bath. Sample temperature was essentially equal to the bath temperature during irradiation and during resistivity measurement. Highest temperatures reached were during filling, when sample and thermometer temperatures were identically equal. During run I, 2.2 K was reached occasionally; during the latter part of run II and throughout runs III and IV, temperature was always kept below 2.0 K. The two samples of a given run were, of course, identically equal in temperature during every fill. For comparison of samples from different runs, we look ahead to Sec. IV and extrapolate the 2.5% thermal recovery per degree below 2.3 K. This gives the uncertain estimate that the ±0.1-K temperature difference between fills would yield ∓0.25% difference in the observed production rate. If this estimate is correct, then differences in thermal anneal between irradiation steps can be neglected.

III. SIZE EFFECT

For low values of resistivity, the electron mean free path becomes comparable to sample dimensions. This size effect serves to increase the measured resisitivity above the bulk value. A review of size effect corrections is given by Sondheimer[16] with a discussion of the objections to size effect theory. Calculations are done by Dingle[17] for round wires and by MacDonald and Sarginson[18] for square wires. Birtcher[19] numerically integrated MacDonald and Sarginson's Eq. (5) to show that square wires differ from round wires of equal cross section by less than 2%. Size corrections require the product of bulk resistivity times mean

TABLE II. Data obtained in run I. Φ is the electron fluence, $\Delta\rho$ is the change in electrical resistivity from the initial unirradiated value, $\Delta\rho_B$ is the size-corrected change in resistivity, T_i is the irradiation temperature, and T_a is the annealing temperature. $T_i \leq 2.2$ K; $d\Phi/dt = (0.8\text{–}4.0) \times 10^{12} e/\text{cm}^2$ sec.

T_a (K)	Φ $10^{16} e/\text{cm}^2$	I A $\Delta\rho$ 10^{-9} Ω cm	I A $\Delta\rho_B$ 10^{-9} Ω cm	I Q $\Delta\rho$ 10^{-9} Ω cm	I Q $\Delta\rho_B$ 10^{-9} Ω cm
	0.4942	0.07776	0.077	0.09762	0.0979
	3.076	0.3788	0.395	0.2421	0.2428
18		0.2978	0.305	0.1469	0.1473
	7.489	0.8493	0.905	0.3896	0.3918
24		0.6714	0.710	0.2597	0.2605
	8.920	0.8359	0.890	0.3317	0.3327
4.2		0.8254	0.875	0.3223	0.3233
	9.127	0.8491	0.905	0.3299	0.3309
13		0.8153	0.865	0.3175	0.3185
	9.561	0.8647	0.920	0.3288	0.3298

free path given experimentally[20] $\rho_B l = 1.19 \times 10^{-11}$ Ω cm^2 for gold.

Size effects are calculated according to Sondheimer assuming diffuse scattering of electrons ($p = 0$) by the wire surface. Calculations were done for a round wire 376.9 μm in diameter; the geometrical factor for a 7.62-cm length of this wire is the same as that for sample III A (see Table I). The pure size effect ($\rho_B = 0$) is 0.3157×10^{-9} Ω cm, to be compared to the measured residual resistivity 0.3837×10^{-9} Ω cm of sample III A (Table I). The difference ($\rho_B = 4.9 \times 10^{-11}$ Ω cm) is attributed to residual impurity resistivity. Hence the size-corrected residual resistance ratio of sample III A is 5.0×10^4 (room-temperature resistivity = 2.44×10^{-6} Ω cm). The corresponding figures for the samples of run II are 5.2 and 7.2×10^4 for samples II L and II H, respectively. For sample I A the ratio is 3.05×10^4.

Exact values of size corrections are not to be taken too seriously, since the 5% uncertainty in the experimental[20] $\rho_B l$ leads to a 5% uncertainty in resistivity (30% uncertainty in size-corrected residual ratios).

TABLE III. Data obtained in run II.
$T_i = 6 \pm 1$ K; $d\Phi/dt = (1.37\text{–}2.74) \times 10^{12} e/\text{cm}^2$ sec

Φ $10^{16} e/\text{cm}^2$	II L $\Delta\rho_L$ 10^{-9} Ω cm	II L $\Delta\rho_B$ 10^{-9} Ω cm	Φ $10^{16} e/\text{cm}^2$	II H $\Delta\rho_H$ 10^{-9} Ω cm	II H $\Delta\rho_B$ 10^{-9} Ω cm
0.03099	0.01099	0.0074	0.06178	0.02009	0.0102
0.1147	0.03162	0.0224	0.8237	0.1099	0.0953
1.530	0.1804	0.1642	2.059	0.1789	0.1629
3.963	0.3122	0.3079	2.510	0.2046	0.1882
			4.471	0.3197	0.3156
			5.657	0.3843	0.3840
			9.590	0.5953	
			15.866	0.8946	
			16.376	0.9168	
$T_a = 78$ K; $T_i \leq 2$ K; $d\Phi/dt = (0.39\text{–}3.13) \times 10^{12} e/\text{cm}^2$					
	0.1608	0.1442		0.5185	
4.060	0.1955	0.1790	16.614	0.5590	
			16.967	0.5842	
			17.140	0.5932	
$T_a = 80$ °C; $T_i \leq 2$ K; $d\Phi/dt = (0.39\text{–}3.13) \times 10^{12} e/\text{cm}^2$					
	0.1064	0.0916		0.2262	0.2092
4.237	0.1557	0.1401	17.317	0.2748	0.2669

TABLE IV. Irradiation data obtained in run III.
$T_i \leq 2.0$ K; $d\Phi/dt = (0.78 \pm 0.04) \times 10^{12} e/\text{cm}^2$.

Φ $10^{16} e/\text{cm}^2$	III A $\Delta\rho$ 10^{-9} Ω cm	III A $\Delta\rho_B$ 10^{-9} Ω cm	Φ $10^{16} e/\text{cm}^2$	III Q $\Delta\rho$ 10^{-9} Ω cm
0.05883	0.02178	0.0197	0.5883	0.04421
0.1177	0.04247	0.0399	0.1177	0.06571
0.1765	0.05711	0.0544	0.1765	0.07792
0.2391	0.06773	0.0648	...	...
0.2942	0.07505	0.0719	0.2951	0.09356
0.4118	0.08750	0.0841	0.4137	0.1070
0.5295	0.09958	0.0962	0.5314	0.1170
0.7129	0.1150	0.1115	0.7115	0.1346
0.8825	0.1311	0.1269	0.8825	0.1468
1.059	0.1457	0.1412	1.059	0.1627
1.236	0.1615	0.1568	1.236	0.1759
1.412	0.1757	0.1706	1.412	0.1905
1.589	0.1918	0.1864	1.589	0.2042
1.706	0.2021	0.1964	1.706	0.2137
1.883	0.2164	0.2107	1.883	0.2269
0.2059	0.2316	0.2259	2.059	0.2394

IV. EXPERIMENTAL RESULTS

A. Resistivity Data

Table I gives a summary of the four runs of this experiment and names each of the two samples in each run. Tables II–V give the measured resistivity changes $\Delta\rho$ and the integrated flux Φ associated with each resistivity change. The flux $d\Phi/dt$ used is given. Temperatures during irradiation are indicated. Also any annealing done during a long irradiation is noted together with the change in resistivity produced by this annealing. $\Delta\rho_B$ is the change in the bulk resistivity.

Run I was a preliminary experiment in which two samples, one well annealed and one quenched, were irradiated and annealed together several times in succession. Beam flux was varied to balance the flow of liquid helium through the needle

TABLE V. Irradiation data obtained in run IV.
$T_i \leq 2$ K; $d\Phi/dt = (0.78 \pm 0.04) \times 10^{12} e/\text{cm}^2$ sec.

Φ	IV 0.01Ag $\Delta\rho$ 10^{-9} Ω cm	IV 0.1Ag $\Delta\rho$ 10^{-9} Ω cm
0.05883	0.01857	0.02924
0.1177	0.03319	0.04874
0.5883	0.08099	0.1015
0.9413	0.1075	0.1373

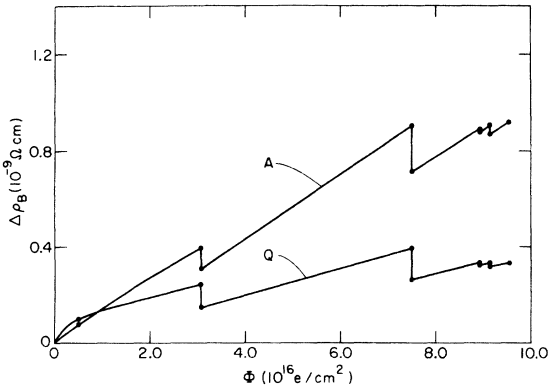

FIG. 8. Change in size-corrected resistivity $\Delta\rho_B$ vs integrated flux Φ for irradiation with 2.5-MeV electrons below 1.8 K. Beam flux was varied $(0.8–4)\times10^{12}e/cm^2$ sec. Two samples irradiated together: sample A well annealed and sample Q quenched from 900 °C. Five irradiations separated by four anneals to temperatures indicated. Occasional anneals to 2.2 K not indicated. Run I.

valve (Sec. IIB2). Beam distribution between the two samples was 50–50±10% (Sec. IIC1). Irradiation temperature increased with increasing beam flux (maximum value 1.8 K). With the beam off, the refrigerator reservoir occasionally overfilled, warming the samples to 2.2 K. The results are shown in Fig. 8.

Run II consisted of two parts. In the first part, a high-radiation dose was introduced at elevated temperatures. As in run I, both samples were irradiated together, but beam distribution was measured by occasionally shuttering sample L. Only in this part, sample heating by the beam was allowed to run ahead of the liquid-helium flow through the needle valve. Thus the sample was cooled by a few mm pressure of He gas at 2 K. Actual sample temperature was 6 K. In the second part, the samples were irradiated below 1.75 K and kept below 2 K during helium fills. The effects of radiation history, dose, and dose rate were studied. [The irradiation results for run II are shown in Figs. 9(a) and 9(b).]

In run III, a well-annealed sample and a quenched sample were irradiated. Beam flux was $0.78\times10^{12}e/cm^2$ sec throughout. Irradiation proceeded in steps of $0.059\times10^{16}e/cm^2$ per step with a helium refill below 2 K at each step. Shutters were used (Fig. 7) in order to irradiate one sample at a time, alternating from sample to sample with each step. Resistivity measurements were taken after each step early in the experiment, and after every two or three steps later. The data are plotted in Fig. 10.

In run IV, two silver-doped samples were irradiated. Irradiation procedure was identical to run III. The results are plotted in Fig. 11.

B. Production Rate Data

Production rate data are derived from the resistivity data. In run I, Table II, the integrated flux between the 18 and 24 K anneals is $7.489-3.076=4.413\times10^{16}e/cm^2$. The corresponding change in resistivity for sample A is $0.8493-0.2978=0.5515\times10^{-9}\,\Omega\,cm$. Dividing the latter by the former yields the average production rate $1.25\times10^{-26}\Omega\,cm^3/e$. Similarly, the average production rate for the same radiation interval in sample Q is $0.55\times10^{-26}\,\Omega\,cm^3/e$. Consideration of the precision to which resistivity was measured in run I gives uncertainties of ±0.25 and 0.11, respectively, for these two numerical results. Production rate results are plotted in Figs. 12 and 13.

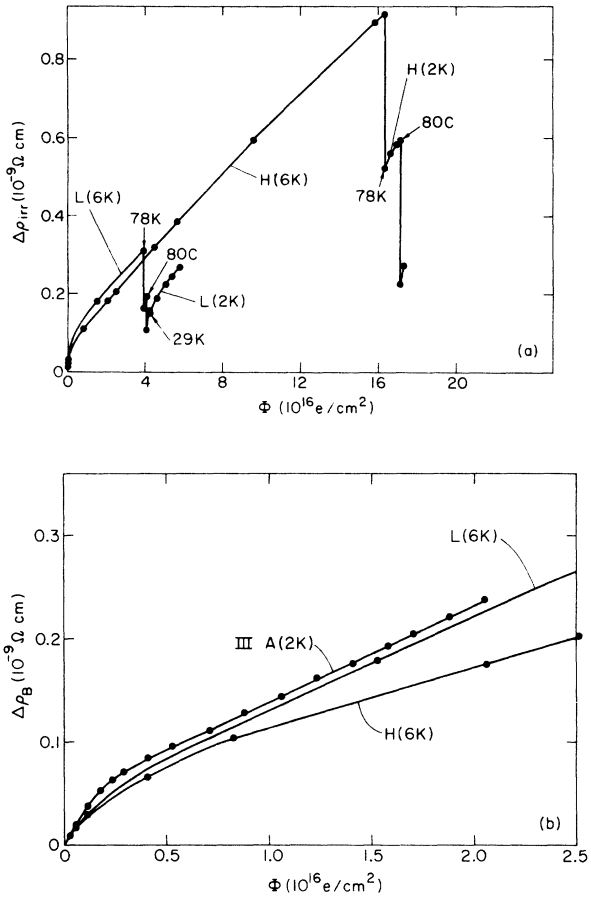

FIG. 9. Change in resistivity $\Delta\rho$ vs integrated flux Φ for irradiation with 2.5-MeV electrons. Sample temperature 6 ± 1 K before 78 K anneal, ≦2 K after 78 K anneal. Beam flux varied (generally higher in sample L $(0.4–3.9)\times10^{12}e/cm^2$ sec. Three anneals to temperatures indicated. Sample L low dose and sample H high dose, run II. (a) Complete data; (b) low Φ region size corrected with sample III A included for comparison.

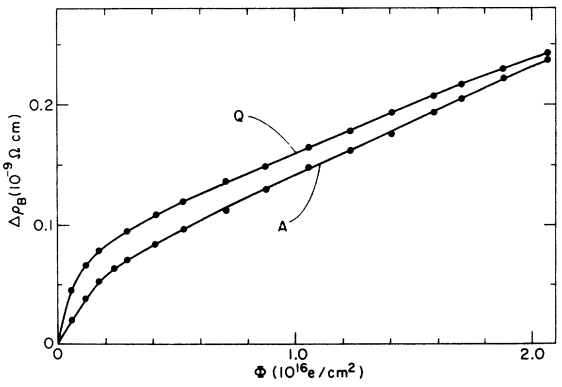

FIG. 10. Change in size-corrected resistivity $\Delta\rho_B$ vs integrated flux Φ for irradiation with 2.5-MeV electrons at 1.55 ± 0.05 K. Anneals at each point due to refrigerator filling with beam off at $T \leq 1.95$ K. Sample A well annealed and sample Q quenched from 600 °C. Samples irradiated alternately with 0.78×10^{12} e/cm^2 sec. Run III.

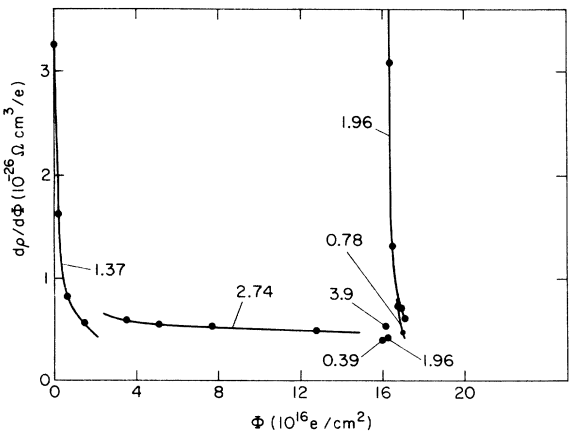

FIG. 12. Production rate $d\rho/d\Phi$ vs integrated electron flux Φ. Derived from data of run II, sample H. Beam flux $d\Phi/dt$ indicated in units of $10^{12}e/\mathrm{cm}^2$ sec, ± 5% accuracy. Sample was annealed at $16.4 \times 10^{16}e/\mathrm{cm}^2$ to 78 K.

C. Size Effect Corrections

As stated in Sec. III, measured resistivity values ρ must be corrected to give equivalent bulk resistivity values ρ_B. For sample IIIA, where these size effects are considerable, the size-corrected resistivity data results are given in Table IV. For production rate data we use

$$\frac{d\rho_B}{d\Phi} = \frac{d\rho_B}{d\rho}\,\frac{d\rho}{d\Phi} \quad . \tag{3}$$

This size correction is included in Table IV for sample A, run III. In the case of III Q, the initial (quenched) resistivity of 1.726×10^{-9} Ω cm causes the size corrections to be small. Size corrections of production rate data for run IV are 0.5% and 0.05%, respectively, for samples 0.01 and 0.1.

D. Recovery Data

In run I four different annealing experiments were performed. Prior to the annealing data shown in Fig. 14, the specimen IA had been irradiated to $\Phi = 7.49 \times 10^{16}e/\mathrm{cm}^2$ and annealed to 24 K ($\Delta\rho = 0.6714 \times 10^{-9}$ Ω cm). An additional $\Delta\Phi = 1.431 \times 10^{16}e/\mathrm{cm}^2$ at 2.2 K gave a total $\Delta\rho = 0.8359 \times 10^{-9}$ Ω cm. The annealing data of Fig. 15 were then obtained.

In run II short irradiations at 2 K after the 78-K anneal for IIH and after the 80 °C anneal for IIL gave small increases in resistivity. A subsequent anneal at 4.2 K produced decreases in resistivity

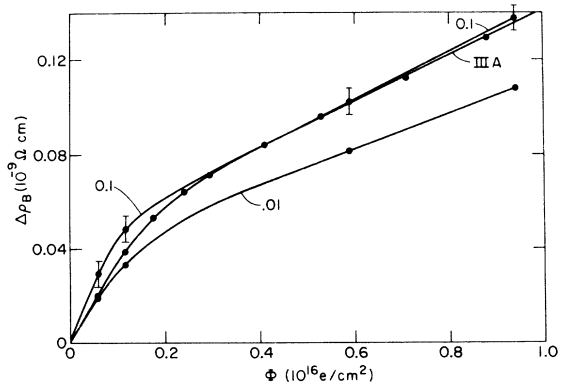

FIG. 11. Change in resistivity $\Delta\rho_B$ vs integrated flux Φ for run IV. Same irradiation conditions as in run III. Two samples doped with 0.01- and 0.1-at.% silver, respectively. Error in sample 0.1 due to large initial resistivity. Sample IIIA data included for comparison.

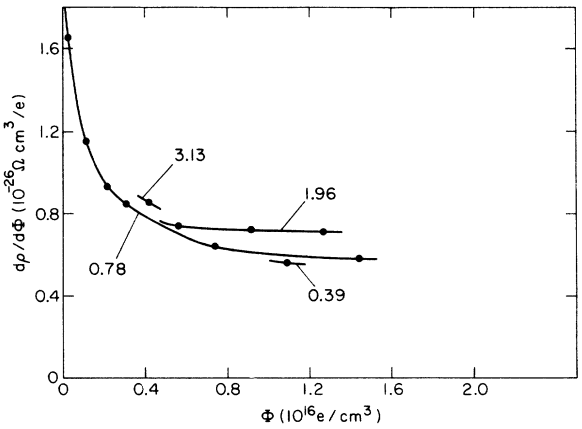

FIG. 13. Production rate $d\rho/d\Phi$ vs integrated electron flux Φ. Derived from the data of run II, sample L, immediately after the 29 K anneal. Beam flux $d\Phi/dt$ alternated among the four values indicated in units of $10^{12}e/\mathrm{cm}^2$ sec, ± 5% accuracy.

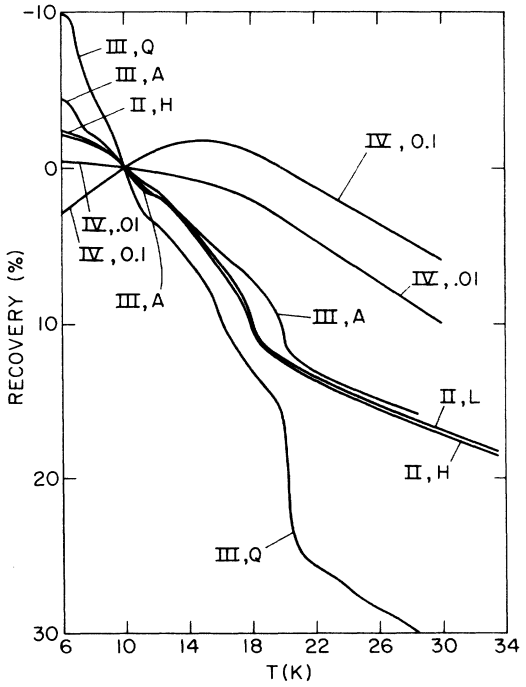

FIG. 14. Isochronal-recovery data, normalized to 10 K. 3.0-min steps, 40 steps per decade. Accuracy: Runs II and III, ≅ line thickness; run IV, 0.01—1%; run IV, 0.1—7%.

in both specimens.

In run III isochronal annealing was done at a series of temperatures from 5.33 K and up. The results are shown in Fig. 16.

A survey of the annealing results is shown in Fig. 14. The results for II H and II L were obtained after the 6 K irradiation.

V. SUMMARY OF EXPERIMENTAL RESULTS

The curves of $\Delta\rho_B$ vs Φ for annealed, quenched, and silver-doped specimens are curved. The production rate for resistivity decreases as Φ increases.

The curves of $\Delta\rho_B$ vs Φ for quenched specimens at first lie above the curves for annealed specimens. Finally as Φ increases above 1 or 2 $\times 10^{16} e/\text{cm}^2$ the curves cross.

The production rate $d\rho/d\Phi$ for given Φ can be increased slightly by increasing the beam flux $d\Phi/dt$. For example, increasing $d\Phi/dt$ from 0.39 $\times 10^{12} e/\text{cm}^2$ sec to $1.96\times 10^{12} e/\text{cm}^2$ sec at $\Phi = 1.1 \times 10^{16} e/\text{cm}^2$ increases the production rate from $0.561\times 10^{-26}\ \Omega\,\text{cm}^3/e$ to $0.719\times 10^{-26}\ \Omega\,\text{cm}^3/e$.

Annealing of $\Delta\rho_B$ is observed in annealed and quenched specimens in the range 2–5.33 K.

Upon annealing to given temperature larger changes in $\Delta\rho_B$ are seen in the quenched specimens than in the annealed specimens.

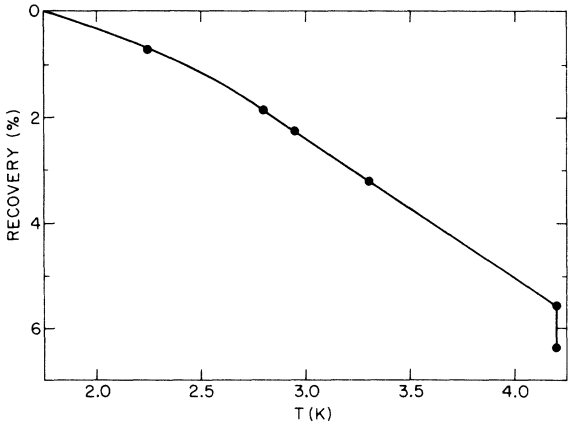

FIG. 15. Recovery of resistivity vs temperature for the isochronal anneal to 4.2 K of run I, sample A.

The damage production data for the silver-doped specimens is confusing since the 0.01-at.% specimen shows an abnormally low curve of $\Delta\rho_B$ vs Φ whereas the 0.1-at.% specimen gives a $\Delta\rho_B$ vs Φ like that of the annealed specimen. Further data are required.

Recovery did not begin until about 19 K in the 0.01-at.% silver specimen.

VI. ASSESSMENT

The experimental findings were given in Sec. V. In contrast to copper and silver the production

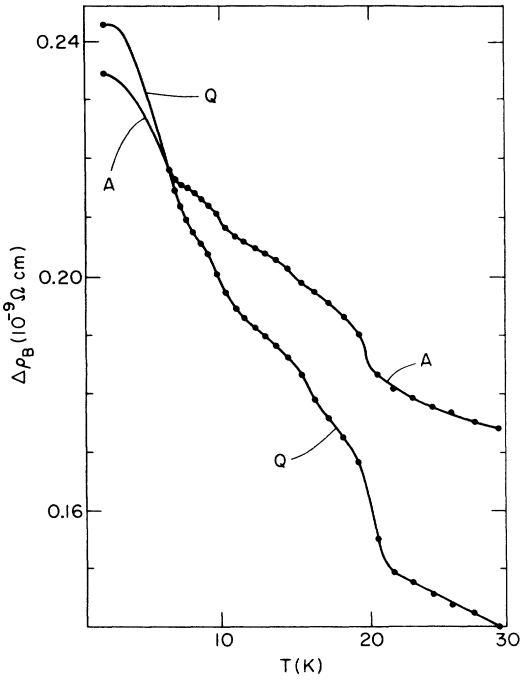

FIG. 16. Size-corrected resistivity vs temperature for isochronal anneal of samples A and Q, run III.

curve at 2 K bends downward. Moreover, the alterations produced by vacancies and impurities on the production curves are complex and not yet understood. The fact that annealing begins upon warming to 2.5 K suggests that the damage is in a very unstable state. Since no transients were observed at 2 K, one has the feeling that whatever defect migration is required to give a precarious stability at 2 K has already occurred. Perhaps the electron beam causes some migration.

There are a number of questions not resolved by the present work. The most vexing are the following: (i) We believe that defect migration occurs during irradiation at 2.0 K. Is the migration thermal or does the electron beam cause the migration? In fact, the use of subthreshold irradiation did not cause annealing in a silver-doped sample so that what little evidence we have is negative. (ii) Does the migration occur in one dimension or in three dimensions? (iii) Why is gold so different from copper and silver?

In conclusion, gold behaves very differently from copper and silver upon electron irradiation at 2 K, but as yet one does not understand why.

---

*Work supported by Army Research Office, Durham, North Carolina.

[1]H. G. Cooper, J. S. Koehler, and J. W. Marx, Phys. Rev. **97**, 599 (1955).
[2]J. B. Ward and J. W. Kauffman, Phys. Rev. **123**, 90 (1961).
[3]W. Bauer, J. W. DeFord, and J. S. Koehler, Phys. Rev. **128**, 1497 (1962).
[4]H. C. Cooper, R. B. Smith, and R. M. Walker, Phys. Rev. **114**, 1452 (1959).
[5]H. C. Cooper, R. B. Smith, and R. M. Walker, Phys. Rev. **114**, 1460 (1959).
[6]R. R. Coltman, C. E. Klabunde, and J. K. Redman, Phys. Rev. **156**, 715 (1967).
[7]W. Schilling, G. Burger, K. Isebeck, and H. Wenzl, in *Vacancies and Interstitials in Metals*, edited by A. Seeger, D. Schumacher, W. Schilling, and J. Diehl (North-Holland, Amsterdam, 1970), p. 255.
[8]R. E. McKeighen and J. S. Koehler, Phys. Rev. B **4**, 462 (1971).
[9]P. S. Gwozdz and J. S. Koehler, Phys. Rev. B **6**, 4571 (1972).
[10]N. F. Mott and H. Jones, *Metals and Alloys* (Dover, New York, 1958), p. 274.
[11]J. W. Corbett in *Solid State Physics*, edited by F. Seitz and D. Turnbull (Academic, New York, 1966), Vol. 7, Chap. 6.
[12]M. J. Berger and S. M. Seltzer, *Tables of Energy Losses and Ranges of Electrons and Positrons* (NASA Scientific and Technical Information Division, Washington, D. C., 1964).
[13]A. C. Rose-Innes, *Low Temperature Techniques* (Van Nostrand-Reinhold, New York, 1964).
[14]*Handbook of Chemistry and Physics*, 53rd ed. (CRC Press, Cleveland, 1972), p. E10.
[15]G. L. Pollack, Rev. Mod. Phys. **41**, 48 (1969).
[16]E. H. Sondheimer, Adv. Phys. **1**, 1 (1952).
[17]R. B. Dingle, Proc. R. Soc. A **201**, 545 (1950).
[18]D. K. MacDonald and K. Sarginson, Proc. R. Soc. A **203**, 223 (1950).
[19]R. Birtcher (private communication).
[20]R. G. Chamber, Proc. R. Soc. A **215**, 481 (1952).

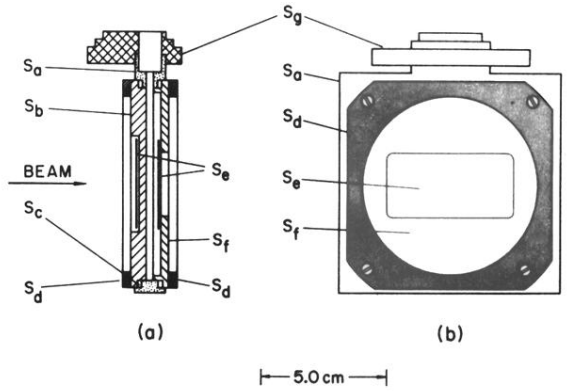

FIG. 5. Sample chamber. (a) Vertical cross section through center. (b) View looking up beam direction. (S_a) Chamber support (gold-plated copper); (S_b) sample mounting plate with two samples not visible in cross section; (S_c) 1.6 mm diameter indium O-rings (two) compressed to rectangular dimensions of grooves; (S_d) stainless-steel pressure rings (two); (S_e) aluminum-foil windows (two) with attachment plates not drawn for clarity; (S_f) cover plate; (S_g) gold-plated copper male flange, soft soldered to chamber support, for attachment to superfluid helium reservoir.